

Optical Engineering

OpticalEngineering.SPIEDigitalLibrary.org

Comparison of absolute low-spatial frequency surface figure measurement for spherical surfaces

Wei-Cheng Lin
Shenq-Tsong Chang
Hua-Lin Chen
Yu-Wei Lin
Chung-Ying Wang
Cheng-Kuo Sung

SPIE.

Wei-Cheng Lin, Shenq-Tsong Chang, Hua-Lin Chen, Yu-Wei Lin, Chung-Ying Wang, Cheng-Kuo Sung, "Comparison of absolute low-spatial frequency surface figure measurement for spherical surfaces," *Opt. Eng.* **59**(6), 064102 (2020), doi: 10.1117/1.OE.59.6.064102

Comparison of absolute low-spatial frequency surface figure measurement for spherical surfaces

Wei-Cheng Lin,^{a,*} Shenq-Tsong Chang,^a Hua-Lin Chen,^a Yu-Wei Lin,^a
Chung-Ying Wang,^a and Cheng-Kuo Sung^b

^aTaiwan Instrument Research Institute, National Applied Research Laboratories,
Hsinchu, Taiwan

^bNational Tsing Hua University, Department of Power Mechanical Engineering,
Hsinchu, Taiwan

Abstract. Optical metrology is a critical and complex technique for the fabrication of precision optics in which the surface figure is better than peak-to-valley $1/10\lambda$ or RMS $1/30\lambda$. Careful calibration of the intrinsic system errors of the experimental setup, including the alignment error of the metrology tool and the manufacturing error of the reference optics, should be performed. However, any surface deformation caused by the mounting supporter or a gravity effect can result in an incorrect surface figure correction, especially in mid-to-large optics. The system error of the experimental setup and deformation by external conditions of the optics, such as temperature drift, air turbulence, and vibration, affect the measured result. In the proposed method, the magnitude and phase of all nonrotationally symmetrical Zernike coefficients were obtained through multiple measurements by rotating the optics. These coefficients were used to analyze absolute low-spatial frequency figures. To verify the reproducibility of the proposed method, three metrology tools with distinct measurement methods were used to obtain surface figures and the results were then compared. © The Authors. Published by SPIE under a Creative Commons Attribution 4.0 Unported License. Distribution or reproduction of this work in whole or in part requires full attribution of the original publication, including its DOI. [DOI: [10.1117/1.OE.59.6.064102](https://doi.org/10.1117/1.OE.59.6.064102)]

Keywords: absolute measurement; intrinsic system error; Zernike coefficient; phase-shifting Fizeau interferometer; instantaneous phase-shifting Fizeau interferometer; Shack–Harmann wavefront sensor.

Paper 20200162 received Feb. 12, 2020; accepted for publication May 14, 2020; published online Jun. 2, 2020.

1 Introduction

Currently, the optical lithography projection lenses used in the lithography process represent the highest resolution and most accurate optical imaging system.¹ The accuracy of the fabrication technique of optics, particularly aspheric elements, has been significantly improved in the last few years driven by the urgency for breakthroughs in lithography technology.² In the manufacturing process for aspheric optics, optical metrology is a critical and complex technique that is typically tested interferometrically using refractive, diffractive, or hybrid null optics systems.³ The calibration of the intrinsic system error of interferometers and the wavefront error of the attached optics in the interferometry test are typically verified using different techniques. This wavefront error includes errors caused by transmission sphere, computer-generated holograms, or null optics in the experimental setup.⁴ To achieve the desired surface quality for the error budget, several well-known absolute interferometric testing methods for surface figure correction in flat, spherical, and aspherical surfaces have been demonstrated over the years.^{5–9}

Several studies have been conducted to address the error caused by the experimental setup. Careful calibration of the intrinsic systematic error of the experimental setup, including the alignment error of the metrology tool and manufacturing error of the reference optics, is typically performed. However, surface deformations caused by the mounting supporter or gravity effect can result in a misleading judgment for surface figure correction, especially for medium-to-large

*Address all correspondence to Wei-Cheng Lin, E-mail: winstonlin@narlabs.org.tw

optical devices. The system error of the experimental setup and deformation caused by the external conditions of the optical devices, such as temperature drift, air turbulence, and vibration, affect the measured results. To verify the feasibility of the proposed method, three metrology tools (phase-shifting Fizeau interferometer, instantaneous phase-shifting Fizeau interferometer, and Shack–Harmann wavefront sensor) with distinct measuring principles were used for measuring the surface figure to obtain the Zernike coefficients of the 4" spherical lens. According to the proposed approach, the measured results can be analyzed using the phase and magnitude of the absolute surface figure and the system bias constant. The bias constant was primarily caused by the sum of the intrinsic systematic wavefront error from the metrology tool and reference sphere or focusing module. After analyzing the measured result, we concluded that the proposed approach for absolute measurement was in agreement with the nonrotationally symmetric aberration for the spherical surface measured in different environmental conditions and using different measurement tools. We monitored the effect of environmental drift by summarizing the measured data during the measuring period. The instantaneous phase-shifting Fizeau interferometer was used to instantaneously capture the fringes affected by the air turbulence to prevent an error.

2 Description of Absolute Measurement for Spherical Surface

The interferometry test is the measurement of the optical surface figure in which a commercial interferometer with high-quality reference optics (transmission sphere) is used to test the sphere. The traditional test configuration of the concave and convex sphere is shown in Fig. 1(a), and the selection criteria of transmission sphere when measuring the spherical surface are shown in Fig. 1(b).

Typically, the quality for a 1/20 wave at 0.6328 μm of the transmission sphere yields a measurement accuracy of $\sim 1/10$ wave.¹¹ To improve the measurement accuracy, the two-sphere method is widely used with phase-shifting interferometry; it was first described by Jensen¹² and then further studied by Bruning,¹³ Truax,¹¹ and Ellsner et al.¹⁴ In the two-sphere method, a measurement of the cat's eye and multiple measurements at confocal positions are used, and

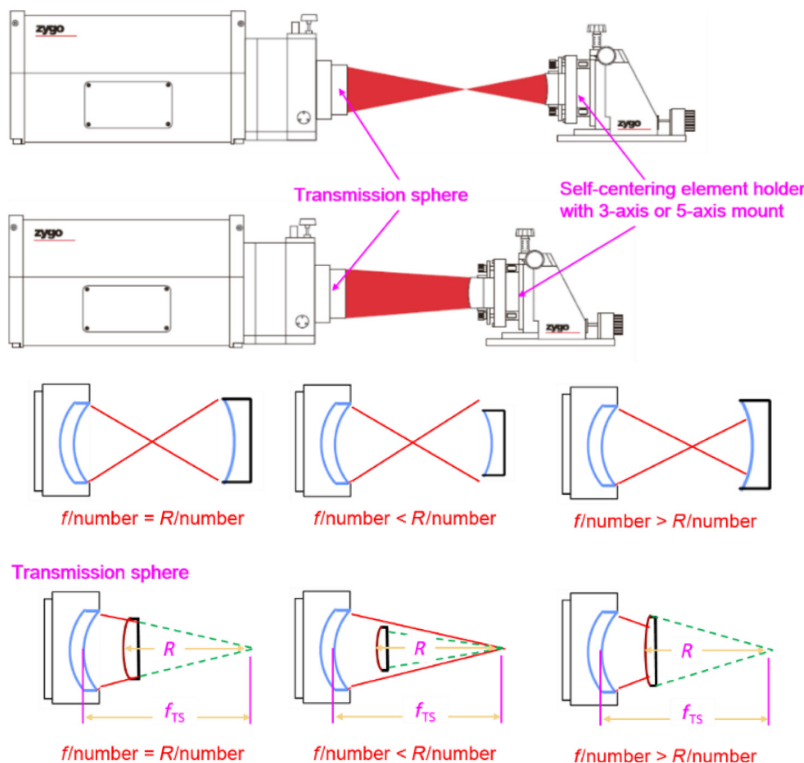


Fig. 1 Schematic of transmission sphere selection for the interferometry test.¹⁰

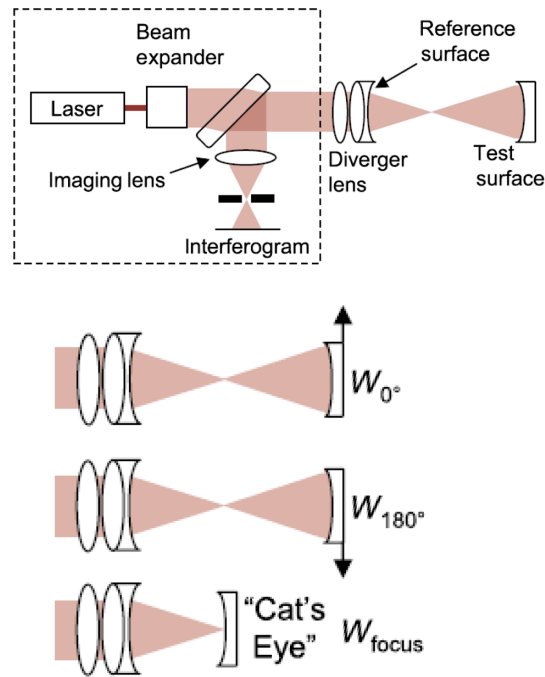


Fig. 2 Measurement setups of the two-sphere method with three positions.³

one of the confocal measurements is obtained after rotating the test surface 180 deg about the optical axis. The cat's eye position allows the measurement of the interferometer without the test sphere. These three measurements are shown in Fig. 2. Moreover, the three main contributing aberrated wavefronts are due to the test surface, the reference arm, and the reference sphere.³

Few studies have examined the two-sphere method with three positions and five positions in detail.¹⁵ The lateral shearing method¹⁶ and shift-rotation method^{17,18} are other approaches that have been widely used in absolute testing for spherical surfaces. Both methods require testing data at multiple positions to separate the surface figure of the test optics from the system error of the interferometer. The lateral shearing method requires testing results at one original position and multiple lateral shifting positions. The shift-rotation method requires testing results at N rotational positions and a lateral shifting position. In this case, high-spatial frequency figure information could not be obtained using the traditional Zernike-based shift-rotation method.

3 Theory and Equipment

3.1 Wavefront and Interferograms

All points on a perfectly spherical wavefront are equidistant from the source such that the optical path difference (OPD) between any two points on this wavefront is zero.¹⁹ For the interferometric test, the interference between the light reflected from the reference and test surface results in the formation of a fringe pattern because of distinct OPDs. Thus, wavefront deviation can be performed using the difference between the two interfering beams that contain information about the aberration level of the test wavefront.³ First, the interferograms were used to calculate the phase map, which was then unwrapped into the wavefront error map (OPD map). Figure 3(a) shows the interferogram and wavefront error map of the optics under test. Generally, wavefront aberration coefficients and Zernike polynomials are two common representations of aberrations that can be used to represent the variations of the actual wavefront from an ideal wavefront. The test wavefront error map obtained from the metrology tool can be divided into two major pieces of information, namely, the map constructed by Zernike polynomial fitting and that residual map that was subtracted from the map of Zernike polynomial fitting from the original wavefront error map, as shown in Fig. 3(b). Zernike polynomials are capable of accurately representing only the

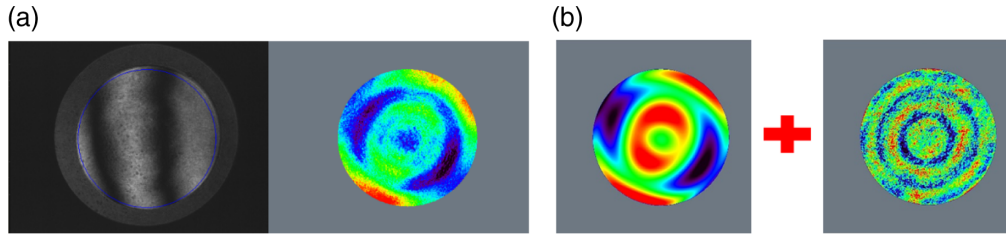


Fig. 3 (a) Demonstration of interferogram (left) and wavefront error map (right) and (b) demonstration of wavefront error map with Zernike polynomial fitting contour and fitting residual.

aberrations inherent to rotationally symmetric optical systems. Therefore, local defects, air turbulence, index variations, and fabrication errors cannot be sufficiently described.³

3.2 Zernike Polynomials

Optical systems generally have an axis of rotational symmetry with a circular or annular pupil. The wave aberration function can be expanded in a power series or a complete set of orthogonal polynomials.²⁰ Wavefront data in polynomial form were used to interpret the optical test results and eliminate typical errors of a lens or lens systems, such as defocus, coma, or astigmatism. Zernike polynomials were first derived by Fritz Zernike in 1934. The polynomials are useful in expressing wavefront data because the shape of these polynomials is the same as that of aberrations. The Zernike polynomials are a set of functions that are orthogonal only in a continuous fashion over the interior of a unit circle in two real variables, radial, r , and azimuthal, θ . Because of the orthogonal property, deleting terms from the set of polynomials or adding terms to the set of polynomials does not affect the value of the remaining or the original coefficients. Therefore, the Zernike polynomial represents an optical surface multiplied by a coefficient and added.

A complete mathematical description for a given surface, $\Delta Z(r, \theta)$, is obtained using the following equation:

$$\Delta Z(r, \theta) = A_{00} + \sum_{n=2}^{\infty} A_{n0} R_n^0(r) + \sum_{n=1}^{\infty} \sum_{m=1}^n R_n^m(r) [A_{nm} \cos(m\theta) + B_{nm} \sin(m\theta)], \quad (1)$$

where A_{nm} and B_{nm} are the Zernike coefficients in the x and y directions, respectively. The radial dependence $R_n^m(r)$ of the Zernike polynomials is obtained using the following equation:

$$R_n^m(r) = \sum_{k=0}^{(n-m)/2} \frac{(-1)^k (n-k)!}{k! [(n+m)/2 - k]! [(n-m)/2 - k]!} r^{n-2k}. \quad (2)$$

The variables m and n in Eqs. (1) and (2) are non-negative integers, and $n \geq m$. For any m , $C \cos[m(\theta - \delta)]$ is expressed as $C \cos[m(\theta - \delta)] = C[\cos(m\theta) \cos(m\delta) + \sin(m\theta) \sin(m\delta)]$; let $A = C \cos(m\delta)$, $B = C \sin(m\delta)$ and $C \cos[m(\theta - \delta)] = A \cos(m\theta) + B \sin(m\theta)$. Each of the Zernike terms is a function of phase angle δ and has a cosine and sinusoidal dependence represented by the Zernike coefficients A and B , respectively. Each pair of terms is expressed as a single term with an associated magnitude C and phase δ as follows:

$$C = \sqrt{A^2 + B^2}, \quad (3)$$

$$\delta = \frac{1}{m} \tan^{-1} \left(\frac{B}{A} \right). \quad (4)$$

3.3 Proposed Approach

The proposed approach can identify the absolute surface figure of nonrotationally symmetric Zernike terms by adopting multimeasurement of the optics rotated with a different orientation

about the optical axis. The range of δ is determined using m in the Zernike polynomial; each Zernike term thus has a distinct characteristic period. Thus, the nonrotationally symmetric parts of the error can be plotted as a sinusoid curve. According to the presented equations in Sec. 3.2, the absolute measurement for the nonrotationally symmetric parts of the error of the measured optics can be distinguished by calculating the magnitude and phase of the fitting curve that was plotted from the results directly obtained when the mirror is rotated. To compare and verify the reproducibility of the absolute measurement in this study, measurement using different equipment was performed.

3.4 Specification of the Equipment

In this study, a concave spherical surface with a peak-to-valley (P-V) 1/10 wave at about 632.8 nm was quantified using interferometric measurements with a Zygo GPI-4" XP Fizeau interferometer and an Engineering Synthesis Design Inc. (ESDI) H1000 instantaneous phase-shifting Fizeau interferometer. Noninterferometric measurement with a HASO R-flex 128 from Imagine Optics was also performed (Fig 4). Brief descriptions of this equipment is summarized.

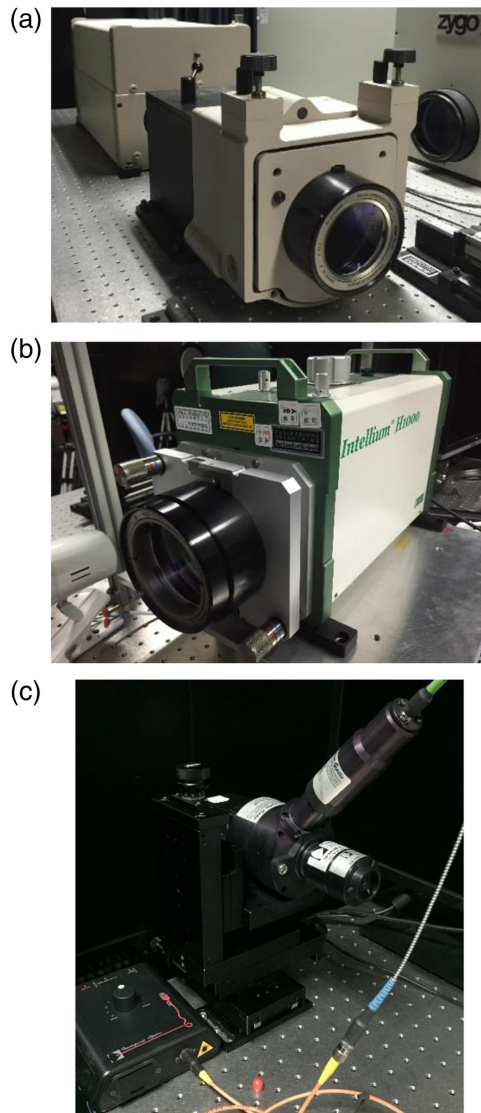


Fig. 4 Description of (a) Zygo GPI-4" XP Fizeau interferometer, (b) ESDI phase-shifting Fizeau interferometer, and (c) HASO R-Flex 128 wavefront sensor.

3.5 Zygo GPI-4" XP Fizeau Interferometer

The model is a phase-shifting interferometer with a digital camera providing a 640×480 resolution for acquisition.

3.6 ESDI Intellium H1000 Phase-Shifting Fizeau Interferometer

This instantaneous phase-shifting Fizeau interferometer is vibration-insensitive and can capture events in the range of $10 \mu\text{s}$. Simultaneous phase-shifting inside Intellium H1000 was performed by a patented I-Phase module to produce three ultraprecise phase-shifted interferograms that were simultaneously acquired.

3.7 HASO R-Flex 128 Wavefront Sensor

HASO R-Flex is a Shack–Harmann wavefront sensor with an autocollimator and a focusing module to provide a versatile and turnkey solution from Imagine Optics. Compared with the Fizeau interferometer, the wavefront sensor exhibited lower spatial frequency but provided higher dynamic range and less sensitivity for environmental conditions such as vibration.

4 Absolute Measurement for Spherical Surface

4.1 Experimental Setup

The sphere was constructed using fused silica with a 4" clear aperture about the P–V 1/10 wave. The F/3.3 reference sphere for the interferometry test with both the Zygo and ESDI Fizeau interferometer and the F/4 focusing module of the noninterferometric test with the HASO R-Flex wavefront sensor were compatible by considering the radius of curvature (440.52 mm) of the optic. Moreover, the optics were attached to an angular polar chart on the backside to determine and control the rotation angle within the absolute measurement. A fixture provided five-axis (x , y , and z axis translation and two-axis tilt about the axis) flexibility, as shown in Fig 5(a). The test configuration for the interferometric test was according to the classical configuration, as shown in Fig. 1. Figure 5(b) shows the interferometric test configuration with the Zygo Fizeau interferometer. The wavefront sensor provided the measurement comparable to the interferometric wavefront testing with direct wavefront measurement. A large NA, high-quality concave spherical mirror with at least a P–V 1/10 wave was used for calibrating the intrinsic systematic alignment error and focusing the module's wavefront. The calibrating configuration and test configuration are depicted in Figs. 5(c) and 5(d), respectively.

4.2 Measured Results of Test Configuration

In this section, the measured results with three test configurations were summarized and compared. Figure 6 shows the wavefront error map for the original orientation of the specified optic measured by the Zygo interferometer, ESDI interferometer, and Haso Shack–Harmann wavefront sensor. We find that the measured result in the P–V value has the maximum difference with 0.5 waves and the RMS value has the maximum difference of a 0.08 wave with each other. In addition, some differences in the orientations and characteristics were observed in the obtained contour map. Because of the differences in the analysis algorithms of these devices, the coordinate system of the presented contour map was reversed to be coincident [Figs. 6(a)–6(c)]. The coordinate system of the wavefront error measured with the Zygo interferometer, ESDI interferometer, and Haso wavefront sensor is shown in Figs. 7(a)–7(c). Moreover, the different operating principles of the interferometer and wavefront sensor provided the inverse of the peak and valley of the contour. Thus, the color labeled blue in the contour map of the wavefront sensor represents the higher area that has the same meaning as the color labeled red in both Zygo and ESDI. To compare the measured results from different equipment, the coordination of the wavefront error map was evaluated. These results were then translated to be coincident.

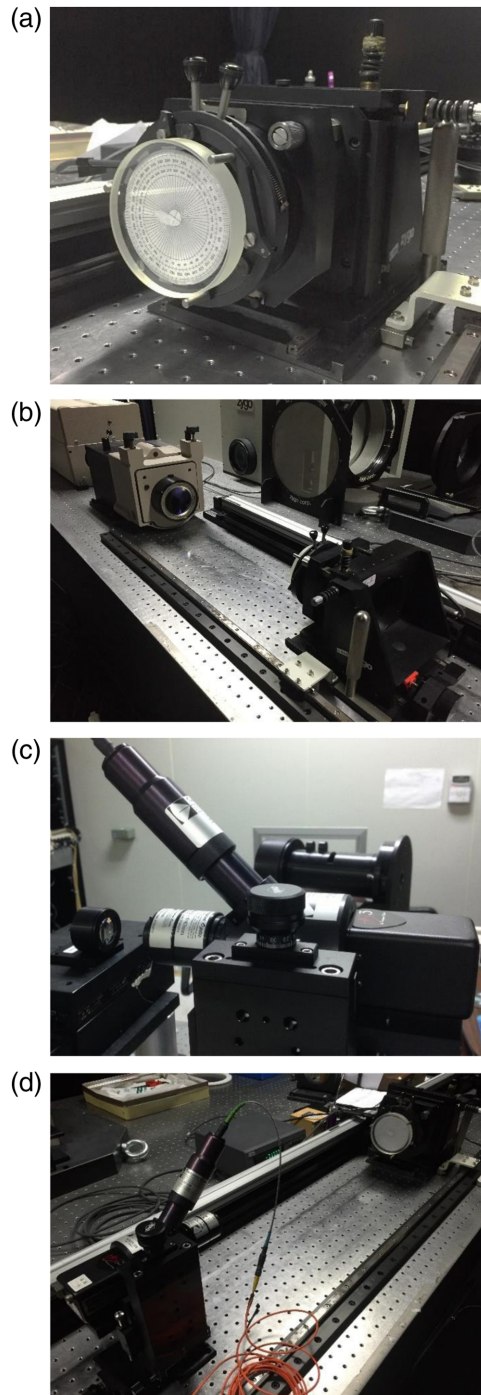


Fig. 5 Illustration of the absolute measurement: (a) optic mounting mechanism, (b) test configuration with interferometer, (c) calibration configuration for the wavefront sensor, and (d) test configuration with wavefront sensor.

In addition, each item of equipment for each test configuration had unique coordination. Before the measured Zernike coefficient was processed, the same coordination was used for the optics under test.

Figures 8(a)–8(c) show the wavefront error map with four of the absolute measurements for 90 deg using Zygo, ESDI interferometer, and HASO wavefront sensor, respectively. The orientation of the contour of the wavefront error map was rotated with the rotation of the test optic. Therefore, the residual form error in the manufacturing process dominates the wavefront that was

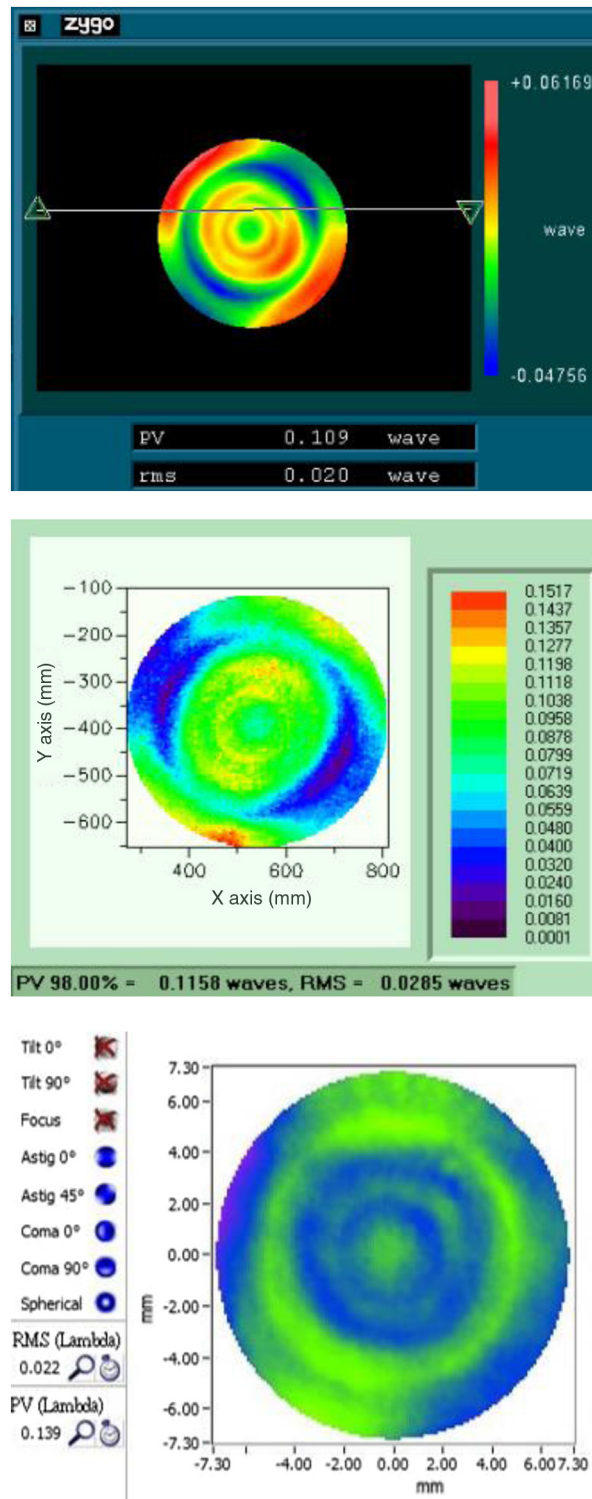


Fig. 6 Demonstration of the wavefront error with each configuration.

measured. Furthermore, Figs. 9 and 10 show the comparison of curve graph plots of the non-rotationally symmetric primary and secondary Zernike coefficient terms when one rotates the spherical lens by 30 deg using Zygo and ESDI interferometer, respectively. Figures 11 and 12 show the comparison of curve graph plots of the nonrotationally symmetric primary and secondary Zernike coefficient terms when one rotates the spherical lens by 30 deg using Zygo

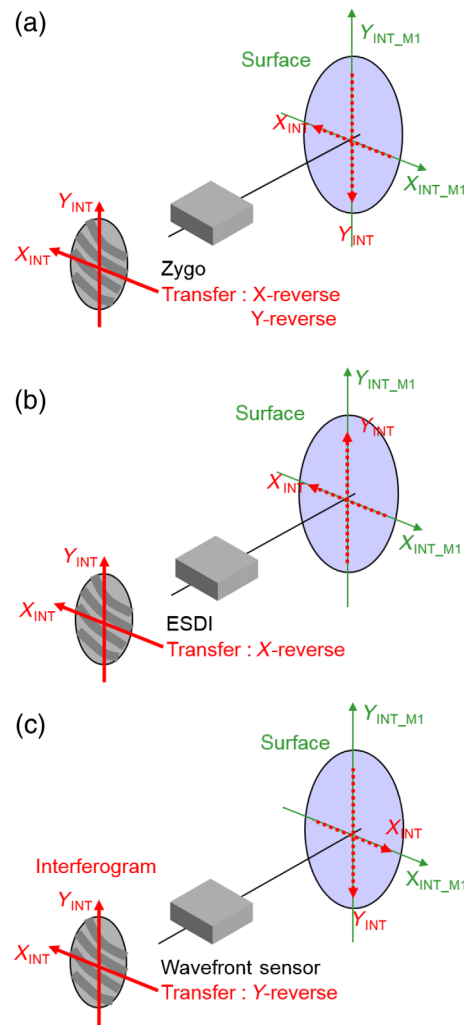


Fig. 7 Coordinate system of the wavefront error measured with (a) Zygo interferometer, (b) ESDI interferometer, and (c) HASO wavefront sensor.

interferometer and HASO wavefront sensor, respectively. The results indicated that the curve plotted from the Zernike coefficient measured with the ESDI interferometer was not similar to that of the sinusoid, especially for the tetrafoil term and of P-V in the range from 0.014 to -0.004 wave. Nevertheless, the Zygo interferometer and wavefront sensor provided reliable and stable measurement, even for the secondary trefoil terms with the magnitude <0.0015 wave (<1 nm). According to Figs. 9 and 10, since some of the plotted curves are not similar to the sinusoid curve, we find that the plotted curve for primary astigmatism between Zygo and ESDI interferometer has almost the same phase and magnitude, but the bias is quite a lot. According to Figs. 11 and 12, we find that the plotted curve for each Zernike term between the Zygo interferometer and the HASO wavefront sensor has almost the same magnitude and a little bias, but there is a constant delay for the phase of each term due to the Zernike polynomial fitting algorithm for the wavefront sensor. As we know, the primary coma term is highly sensitive to the alignment for the optic under test relative to the metrology tool. But we find in Figs. 11 and 12 that the secondary coma term measured from the Zygo interferometer and HASO wavefront sensor is almost perfect to the sinusoid curve even if the magnitude is quite small at 0.003 waves. This phenomenon can be used to prove that the method is less sensitive to the alignment and the Zernike polynomial fitting algorithm is quite robust for further analysis.

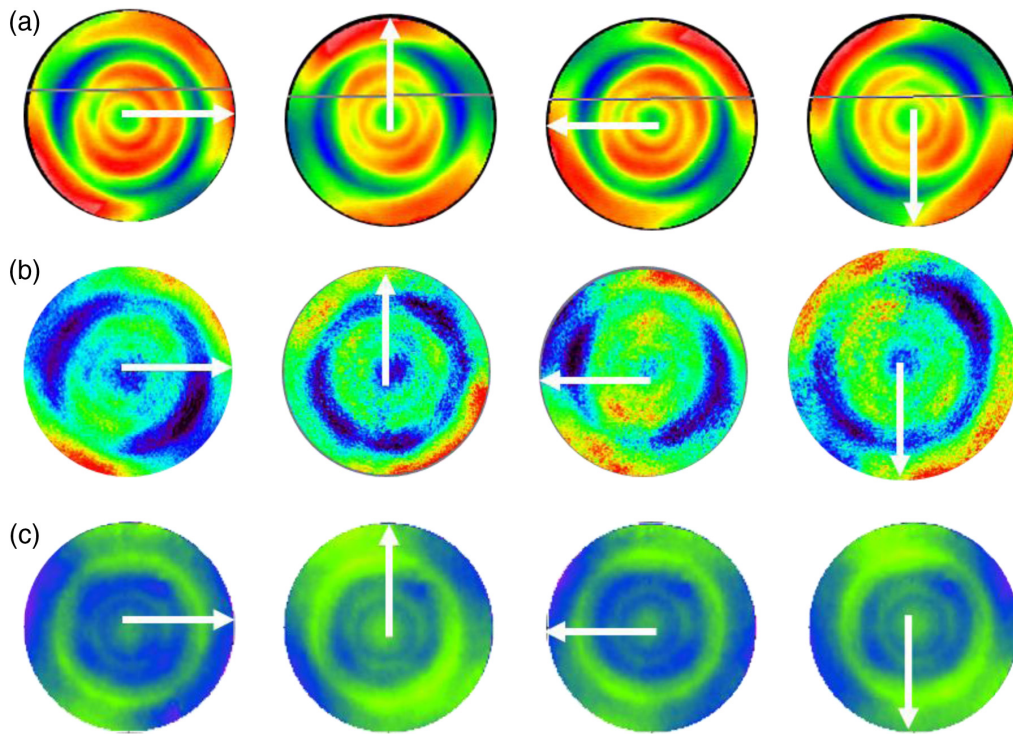


Fig. 8 Wavefront error map of four measurements when rotated by 90 deg using (a) Zygo interferometer, (b) ESDI interferometer, and (c) HASO wavefront sensor.

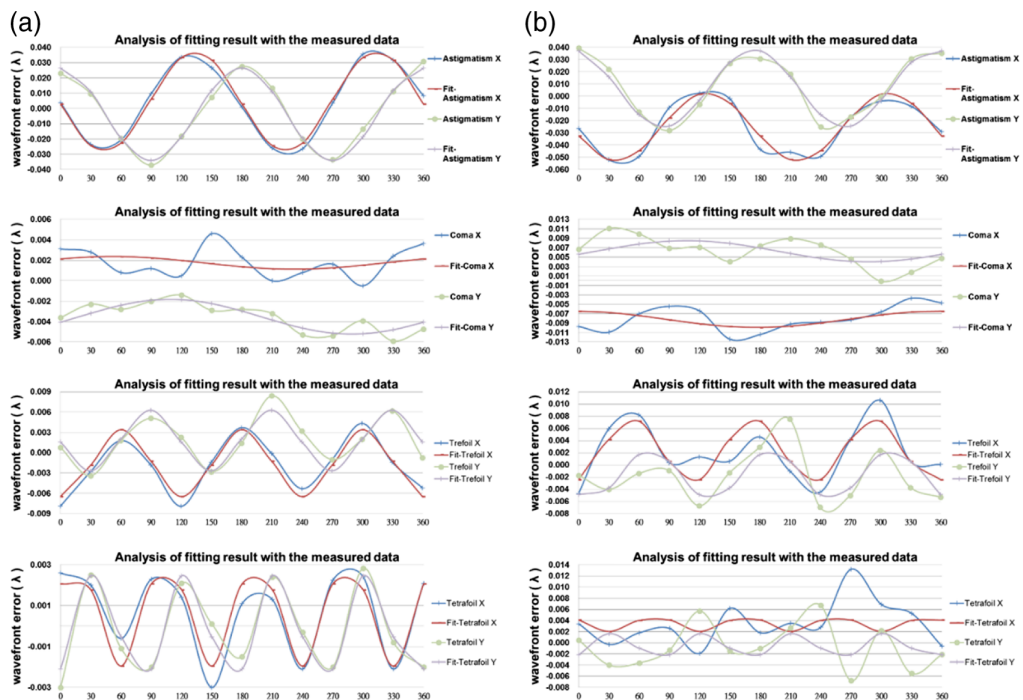


Fig. 9 Comparison of plotted curve of the obtained primary nonrotationally symmetric Zernike coefficient terms when rotating the lens using the Zygo interferometer (a) and ESDI interferometer (b).

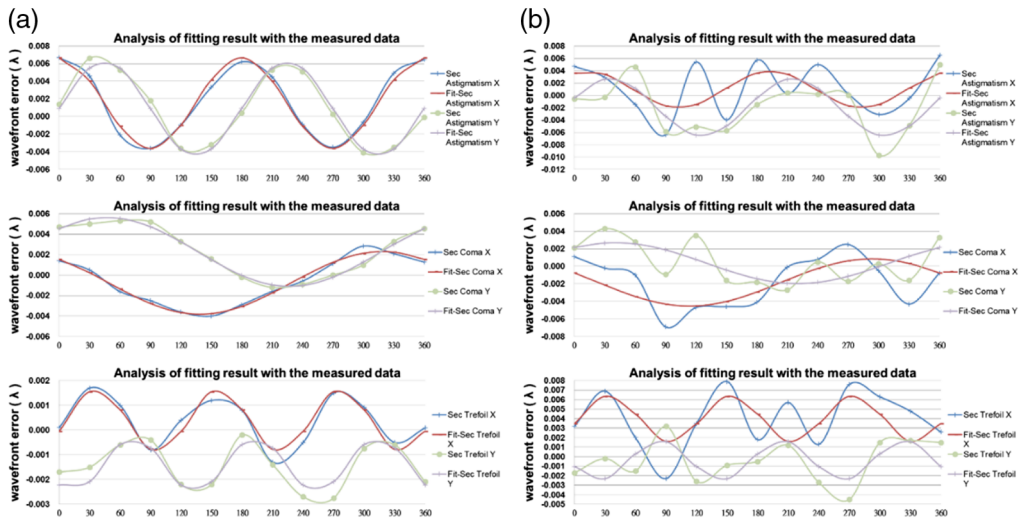


Fig. 10 Comparison of plotted curve of the obtained secondary nonrotationally symmetric Zernike coefficient terms when rotating the lens using the Zygo interferometer (a) and ESDI interferometer (b).

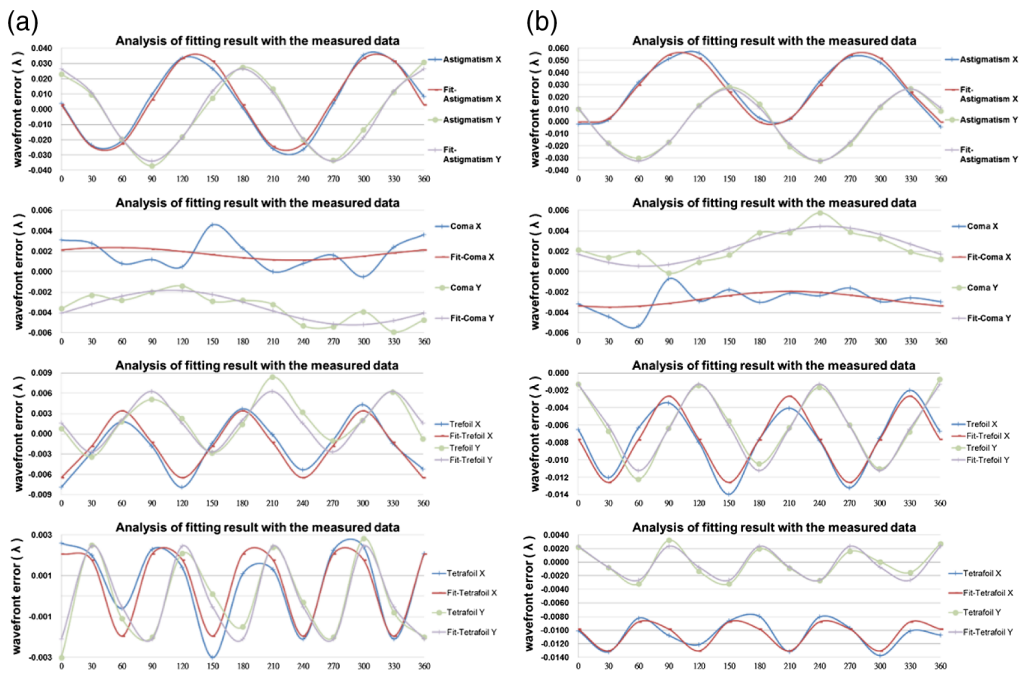


Fig. 11 Comparison of plotted curve of the obtained primary nonrotationally symmetric Zernike coefficient terms when rotating the lens using the Zygo interferometer (a) and HASO wavefront sensor (b).

4.3 Absolute Measurement Analysis

The algorithm between each metrology tool only changes the sign of the Zernike coefficient or the presentation of the peak, valley, and orientation of the contour map. Since the optics under test was rotated, the bias constant was caused by the intrinsic systematic wavefront error for the metrology tool and mounting effect. The measured result was analyzed using the phase and magnitude of the absolute surface figure and system bias constant. The bias constant was primarily caused by the sum of the intrinsic systematic wavefront error from the interferometer, reference sphere, and slight gravity distortion in the interferometric test configuration and

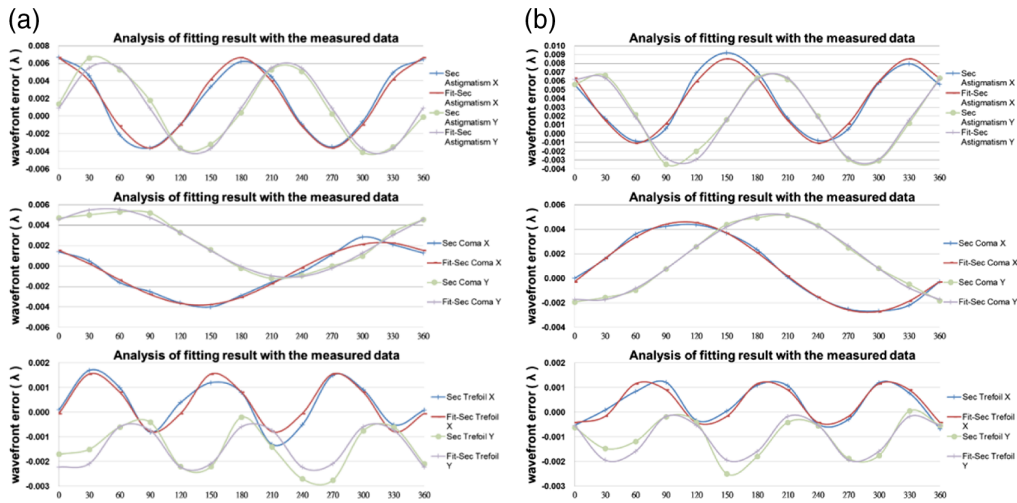


Fig. 12 Comparison of plotted curve of the obtained secondary nonrotationally symmetric Zernike coefficient terms when rotating the lens using the Zygo interferometer (a) and HASO wavefront sensor (b).

the intrinsic systematic wavefront error from the wavefront sensor and focusing module in the noninterferometer test configuration. The analyzed results are shown in Table 1. Although the measured result from the ESDI interferometer exhibited a slight deviation from the theoretical sine or cosine curve, an excellent result can be achieved after fitting. Therefore, the proposed approach for absolute measurement to specify the nonrotationally symmetric aberration provided satisfactory results for the spherical surface.

4.4 Comparison of the Measured Result

As mentioned in the absolute measurement for the sphere, the Zygo interferometer and wavefront sensor provided reliable and stable measurement, even for secondary trefoil terms with magnitudes as low as 0.0015λ (<1 nm). However, the measured result from the ESDI interferometer exhibited a slight deviation from the sinusoid compared with that of the others because the experimental setup in laboratories was different than the environmental conditions, such as temperature control, vibration, and air turbulence. Although satisfactory results after fitting the original data can be achieved, we evaluated the stability and reliability by summarizing the measured data immediately after the optics are rotated for a run. The advantage of the wavefront sensor is that it provides reliable stability that is insensitive to the environment, especially for air turbulence. To find the reason that caused the unsuspected unstable measured results for the ESDI interferometer, we used the wavefront sensor in the same environmental condition as the ESDI interferometer. Then we used the same mounting fixture and repeated the same process for recording the data. The curve plotted with the obtained primary and secondary astigmatism is shown in Fig. 13, which indicates that the curves were not as stable as the measured result used by the wavefront sensor (as shown in Figs. 11 and 12). From the above-mentioned advantage of the wavefront sensor, we assume that the environmental condition for the temperature control of the air conditioning may affect the measured result because the temperature deviation changes the relative position and posture between the optics under test and the metrology tool. Therefore, we used the wavefront sensor to monitor the wavefront error and the temperature sensor to record the deviation of the temperature synchronously. The deviation of temperature compared with focus, astigmatism, spherical aberration, and trefoil together is shown in Fig. 14. The temperature variation with the air conditioning control is about 4°C within 1 h, and the cooling system operates at a beginning temperature of 24°C and remains close to this until the temperature drops to 20°C . It is interesting to note that the rising rate of the temperature is quite the same, so the variation of the temperature is more like a sinusoid curve with a magnitude of about 4°C within 2 h, which is more similar to the phase of the Zernike polynomial. The Zernike coefficient

Table 1 Comparison of the nonrotationally symmetric aberration of the spherical lens.

Form error of lens		Measured with Zygo	Measured with ESDI	Deviation	Measured with Zygo	Measured with HASO	Deviation
Primary astigmatism	Magnitude (wave)	0.031	0.030	-0.001	0.031	0.029	-0.002
	Phase (deg)	45.942	52.496	6.554	45.942	45.918	-0.024
Primary coma	Magnitude (wave)	0.001	0.002	0.001	0.001	0.001	0.000
	Phase (deg)	-35.321	-9.314	26.007	-35.321	-33.825	1.496
Primary spherical aberration	Magnitude (wave)	0.018	0.030	0.012	0.018	0.020	0.002
Primary trefoil	Magnitude (wave)	0.005	0.005	0.000	0.005	0.005	0.001
	Phase (deg)	59.824	-50.278	-110.102	59.824	59.619	-0.205
Secondary astigmatism	Magnitude (wave)	0.005	0.004	-0.001	0.005	0.005	0.000
	Phase (deg)	0.176	-1.268	-1.443	0.176	-1.470	-1.645
Secondary coma	Magnitude (wave)	0.003	0.003	-0.001	0.003	0.003	0.000
	Phase (deg)	41.913	54.398	12.485	41.913	39.859	-2.054
Secondary spherical aberration	Magnitude (wave)	0.000	0.008	0.008	0.000	0.004	0.004
Primary tetrafoil	Magnitude (wave)	0.003	0.002	-0.001	0.003	0.003	0.000
	Phase (deg)	-13.274	-3.994	9.279	-13.274	-12.213	1.061
Secondary trefoil	Magnitude (wave)	0.001	0.002	0.001	0.001	0.001	0.000
	Phase (deg)	-39.956	-42.184	-2.228	-39.956	-42.906	-2.950
Tertiary astigmatism	Magnitude (wave)	0.000	0.001	0.000	0.000	0.000	0.000
	Phase (deg)	24.235	31.017	6.782	24.235	26.035	1.800

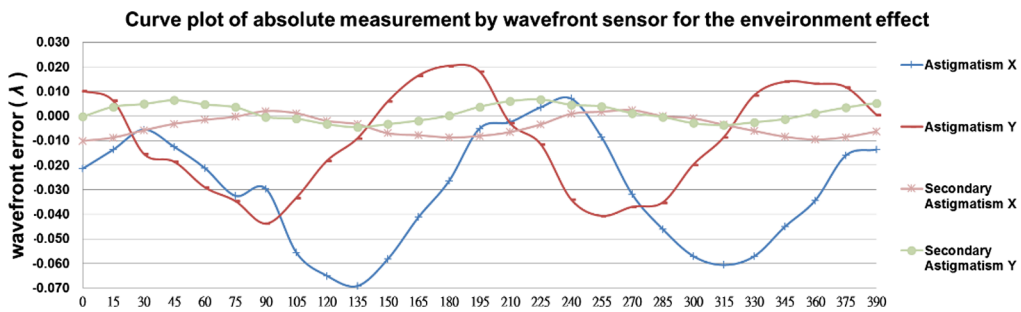


Fig. 13 Measured data using the wavefront sensor in the same environmental condition with the ESDI interferometer.

changed with the same phase of the temperature deviation. Hence, we can conclude that the temperature variation may also affect the measured result and should be monitored carefully. In the proposed method, we observe the real-time variation while plotting the curve by rotating the optics with different orientations to check if the measurement is stable or not.

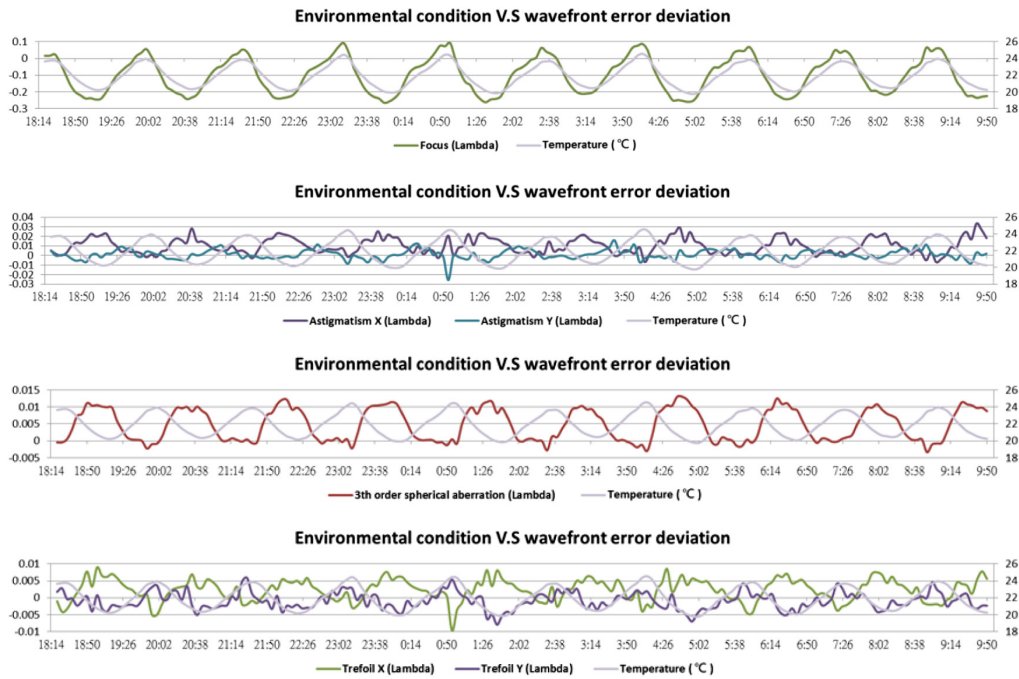


Fig. 14 Comparison of the deviation of temperature with focus, astigmatism, spherical aberration, and trefoil.

5 Results

The proposed approach can identify the absolute surface figure of nonrotationally symmetric Zernike terms based on the characteristic azimuthal spatial frequency of nonrotationally symmetric Zernike terms, excluding the spherical aberration term, which can be calibrated using the random ball test. Unlike previous studies in the literature, this approach also provided excellent classification of the system error contributed by the equipment and the external error source in the test configuration. As long as the mounting mechanism of the optics rotated along the optical axis and environmental conditions within the whole measurement were both stable, the measured result would be more accurate.

6 Conclusions

We conclude that the proposed approach for absolute measurement provided good agreement to the nonrotationally symmetric aberration for the spherical surface measured even in different environmental conditions and with different measurement tools. We monitored the effect of the environment drift by summarizing the measured data during the measured period, preventing a misleading effect that would have happened with the instantaneous phase-shifting Fizeau interferometer when it instantaneously measured the fringes affected by the air turbulence.

Acknowledgments

This work was supported financially by the Ministry of Science and Technology, Taiwan, under Grant Nos. MOST 108-2622-E-492-003-CC3 and MOST 107-2218-E492-009. The experiments were also supported by Taiwan Instrument Research Institute of NARLabs in Taiwan. Also, we thank SPIE Optifab 2019 for publishing the paper based on this research, which was titled “An effective way to calibrate the external errors which are contributed in the interferometric test for spherical surfaces” in conference proceedings.

References

1. J. H. Bruning, "Optical lithography: 40 years and holding," *Proc. SPIE* **6520**, 652004 (2007).
2. V. Bakshi, *EUV Lithography*, SPIE Press and John Wiley & Sons, Inc., Washington (2008).
3. E. P. Goodwin and J. C. Wyant, *Field Guide to Interferometric Optical Testing*, SPIE Press, Bellingham, Washington (2006).
4. F. Schillke, "Critical aspects of testing aspheres in interferometric setups," *Proc. SPIE* **3739**, 317–324 (1999).
5. B. E. Truax, "Absolute interferometric testing of spherical surfaces," *Proc. SPIE* **0966**, 130–137 (1988).
6. K. Creath and J. C. Wyant, "Testing spherical surfaces: a fast, quasi-absolute technique," *Appl. Opt.* **31**, 4350–4354 (1992).
7. R. E. Parks, "Removal of test optics errors," *Proc. SPIE* **0153**, 56–63 (1978).
8. C. J. Evans and R. N. Kestner, "Test optics error removal," *Appl. Opt.* **35**(7), 1015–1021 (1996).
9. G. Seitz, "Absolute interferometric measurement of non rotational symmetric surface errors," in *DGaO Proc.*, P. R. Yoder, Ed., Opto-Mechanical Systems Design, Marcel Dekker Inc., New York, pp. 21–31 (2005).
10. Zygo Corporation, *Transmission Sphere Selection*, Middlefield, Connecticut (2014).
11. B. E. Truax, "Absolute interferometric testing of spherical surfaces," *Proc. SPIE* **1400**, 61 (1991).
12. A. E. Jensen, "Absolute calibration method for Twyman–Green wavefront testing interferometers," *J. Opt. Soc. Am.* **63**, 1313A (1973).
13. J. Bruning, "Fringe scanning interferometers," in *Optical Shop Testing*, D. Malacara, Ed., p. 409, Wiley, New York (1978).
14. K. E. Elssner et al., "Absolute sphericity measurement," *Appl. Opt.* **28**, 4649–4661 (1989).
15. X. Hou et al., "Comparative experimental study on absolute measurement of spherical surface with two-sphere method," *Opt. Lasers Eng.* **49**, 833–840 (2011).
16. E. E. Bloemhof, "Absolute surface metrology by differencing spatially shifted maps from a phase-shifting interferometer," *Opt. Lett.* **35**, 2346–2348 (2010).
17. D. Su et al., "Absolute surface figure testing by shift-rotation method using Zernike polynomials," *Opt. Lett.* **37**, 3198–3200 (2012).
18. W. Song et al., "Optimized absolute testing method of shift-rotation," *Appl. Opt.* **52**, 7028–7032 (2013).
19. M. Tricard, G. Forbes, and P. Murphy, "Subaperture metrology technologies extend capabilities in optics manufacturing," *Proc. SPIE* **5965**, 59650B (2005).

Wei-Cheng Lin received his doctor's degree in physics from the Department of Power Mechanical Engineering, National Tsing Hua University. He is currently an associate engineer at Taiwan Instrument Research Institute, National Applied Research Laboratories. His research interests are optomechanical design, optomechanical system assembly, coordinate measuring machines (CMM) measurement, and optical testing.

Shenq-Tsong Chang received his master's degree in physics from the Catholic University of America. He is currently an associated researcher at Instrument Technology Research Center, National Applied Research Laboratories. His research interests are optical design, CMM measurement, optical testing, and performance evaluation of optical systems.

Hua-Lin Chen received his master's degree in the Department of Mechanical Engineering, National Center University. She is currently an assistant engineer at Taiwan Instrument Research Institute, National Applied Research Laboratories. Her research interests are optomechanical design, vibration and noise signal analysis, and atmospheric pressure plasma researched.

Yu-Wei Lin received his doctor of philosophy degree from the Department of Engineering and System Science at National Tsinghua University. He is currently a research fellow and division director at Taiwan Instrument Research Institute, National Applied Research Laboratories. His research interests are optical testing, vacuum technology, and deposition process.

Chung-Ying Wang received his master's degree from the Department of Mechanical Engineering, National Chung Hsing University. He is currently a project research assistant at Taiwan Instrument Research Institute, National Applied Research Laboratories. His research interests are artificial intelligence application in tool condition monitoring (TCM), thermal error prediction, and roughness prediction of optical element.

Cheng-Kuo Sung is currently working as a professor of the Department of Power Mechanical Engineering, National Tsing Hua University. His major research interest involves design and manufacturing.